Nanoscale

Selective Manipulation of Peptide Orientation on Hexagonal Boron Nitride Nanosheets

Journal:	*Nanoscale*
Manuscript ID	NR-COM-01-2021-000609.R1
Article Type:	Communication
Date Submitted by the Author:	01-Mar-2021
Complete List of Authors:	Brljak, Nermina; University of Miami, Department of Chemistry Jin, Ruitao; Deakin University, Institute for Frontier Materials Walsh, Tiffany; Deakin University, Institute for Frontier Materials Knecht, Marc; University of Miami, Department of Chemistry

SCHOLARONE™
Manuscripts

Please do not adjust margins

COMMUNICATION

Selective Manipulation of Peptide Orientation on Hexagonal Boron Nitride Nanosheets

Received 00th January 20xx,
Accepted 00th January 20xx

DOI: 10.1039/x0xx00000x

Nermina Brljak,[a] Ruitao Jin, [b] Tiffany R. Walsh,[b,*,†] and Marc R. Knecht [a,c,*,†]

The bio-recognition capabilities of materials-specific peptides offer a promising route to obtaining and organizing 2D nanosheet materials in aqueous media. Although significant advances have been made for graphene, little is currently understood regarding how to apply this strategy to hexagonal boron nitride (*h*-BN) due to a lack of knowledge regarding peptide/h-BN interactions. Here, one of the few peptide sequences known with affinity for *h*-BN, BP7, is the focus of mutation studies and bio-conjugation. A combination of experimental methods and modeling reveals the importance of Tyrosine in peptide/*h*-BN interactions. This residue is identified as the key anchoring species, which is then leveraged via bio-conjugation of BP7 to a fatty acid to create new interfacial properties. Specific placement of the fatty acid in the bio-conjugate results in dramatic manipulation of the surface-bound biotic overlayer to generate a highly viscoelastic interface. This viscoelasticity is a consequence of the fatty acid binding, which also down-modulates Tyrosine contact to *h*-BN, resulting in presentation of the extended peptide to solution. In this orientation, the biomolecule is available for subsequent bioconjugation, providing new pathways to programmable organization and conjugation of *h*-BN nanosheets in liquid water.

Introduction

Two-dimensional (2D) nanomaterials have become the focal point for a variety of applications in catalysis,[1] bioimaging,[2] sensing[3] and energy[4] due to their outstanding physical and electronic properties. Of these nanomaterials, graphene has had the greatest interest because of its exceptional structural, mechanical, conductive, and thermal properties.[5] Alternatively, hexagonal boron nitride (*h*-BN) is another promising 2D material that is structurally similar to graphene; it comprises a single atomic layer of boron and nitrogen atoms covalently bound in a hexagonal arrangement. From this unique composition and structure, *h*-BN derives a set of intriguing properties, including a wide bandgap of 5.5-5.9 eV,[6] high thermal stability,[7] and great biocompatibility.[8] As a result, *h*-BN is emerging as an ideal nanostructured insulator, which could prove to be transformational for the design biomacromolecule-based sensors and energy harvesting systems. To obtain *h*-BN sheets, biomolecular-based production strategies are intriguing as they allow for highly specific interactions between the insulating material and other device components; however, very little information is presently known regarding how biomolecules interact with the *h*-BN surface, nor how to manipulate these interactions to control the final properties.

Although the interaction of biomolecules with graphene has been well studied, comparatively little information is known about peptides binding to *h*-BN. For instance, biocombinatorial selection methods have been used to identify peptides with affinity for graphene where numerous sequences have been elucidated and their binding to graphene examined,[9] leading to integration of these interfaces into specific applications.[10, 11] Comparatively, the level of information available for *h*-BN binding peptides is substantially limited. To the best of our knowledge, only two peptides, BP1 (LLADTTHHRPWT) and BP7 (VDAQSKSYTLHD) have been identified via biocombinatorial approaches with affinity for BN surfaces.[12] To this end, Hanagata and coworkers identified the sequences using phage display approaches with BN nanospheres (BNNS) as the target surface. Recent work report by Brljak *et al.* used quartz crystal microbalance (QCM) measurements to quantify the free energy of binding for these sequences to *h*-BN, yielding ΔG values of -29.6 ± 0.6 and -29.5 ± 0.3 kJ mol^{-1} for the BP1 and BP7 peptides, respectively.[13] In conjugation with computational modeling, aromatic and aliphatic (Leu and Val) residues were found to have the greatest contact to *h*-BN, while Asp, His, Lys, and Ser were identified as poor binders.

Although these initial studies identified peptides with affinity for *h*-BN and quantified/characterized their binding, the ability to modulate the binding affinity of biomolecules on a 2D surface remains under-explored. In addition, the previous computational results indicated that both the BP1 and BP7 bound to *h*-BN in a flat orientation, which could conceivably give rise to a non-viscoelastic adlayer, consistent with the vast majority of binding arrangements of materials binding peptides on their target surface.[14, 15] Such results are consistent with dissipation energy measurements from the QCM analysis of

[a] *Department of Chemistry, University of Miami, 1301 Memorial Drive, Coral Gables, Florida 33146, United States.*
[b] *Institute for Frontier Materials, Deakin University, Geelong, 3216 VIC, Australia.*
[c] *Dr. J.T. Macdonald Foundation Biomedical Nanotechnology Institute, University of Miami, Miami, Florida 33136, United States.*
† These authors contributed equally.
Electronic Supplementary Information (ESI) available: Peptide conjugation scheme and additional computational details. See DOI: 10.1039/x0xx00000x

Please do not adjust margins

binding, indicating negligible to no dissipation energy, which demonstrates a non-viscoelastic, flat biological adlayer. The ability to modulate this binding configuration could prove to be highly important for nanomaterial production in aqueous media and their eventual applications, yet direct routes to achieve such *a priori* control remain elusive on the vast majority of materials previously studied. By having the ability to modulate the peptide binding motif, dramatic changes in the biointerfacial properties could be achieved that could prove to be pivotal for exerting control over material assembly in three dimensions, reconfiguration of pre-assembled materials into multiple conformations, or modulation of the surface properties (*e.g.* viscoelasticity at biointerfaces – Scheme 1).

Scheme 1. Illustration of possible molecular-scale differences in peptide/surface orientation of lower- and higher-viscoelastic overlayers.

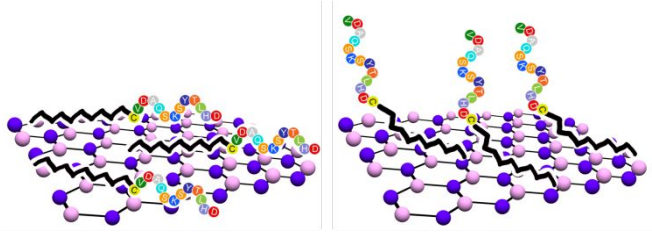

Various modifications to a materials binding peptide could directly influence the surface binding, leading to changes in binding strength, but more importantly the orientation/motif of the biomolecule in the adsorbed state, thus modulating the overall biointerfacial structure. To date, very little knowledge over how integration of non-natural functionalities into peptides affects material binding events is known, which could be used to modulate the structure of surface adsorbed biomolecules.[15] For instance, if the peptides could bind in a vertical orientation, as compared to the horizontal orientation that is typically observed (Scheme 1), this could give rise to new modes of material functionalization. The vertically-bound peptides on the surface would enable a region of the biomolecule to be exposed for secondary modification, analyte binding, integration of additional nanomaterials, etc. This is especially important for 2D nanomaterials such as *h*-BN where this flat interface is ripe for addition of secondary components that remain exceedingly difficult to integrate without chemically disrupting the BN structure, which would lead to defect incorporation. By using the non-covalent attachment of peptides at the interface, integration of secondary components at the *h*-BN surface could be achieved; however, identification of strategies that modulate the surface bound structure of the biomolecules must first be identified.

Herein, through the use of sequence mutations and the integration of fatty acid domains, the ability to interrogate and substantially modify the affinity and surface bound structures of peptides adsorbed to *h*-BN was demonstrated, transforming the in-plane adlayer arrangement of the parent peptide biointerface to a highly viscoelastic biointerface that presents the peptide region to solution. For these studies, the BP7 peptide formed the basis of these modifications, where mutation of key residues identified by Hanagata and colleagues were used to quantitatively confirm both the anchor points to the *h*-BN surface, as well as suspected weak-binding residues in the sequence. This resulted in the ability to switch on and off the binding affinity of the peptide through a single amino acid mutation, which was confirmed via QCM analysis of the binding affinity, in conjunction with Replica Exchange Solvent Tempering Molecular Dynamics (REST-MD) simulations of the surface adsorbed structures of the peptides on *h*-BN. In addition, fatty acid modification of the BP7 sequence at both the N- and C-termini was examined to further modulate the binding affinity and motif. Remarkably, incorporation of the hydrophobic domain at the C-terminus resulted in a highly viscoelastic biointerface at the nanosheet surface. In this arrangement, a substantial fraction of the biomolecules was predicted by modeling to be bound to the *h*-BN surface via the fatty acid domain, presenting the extended peptide to solution. Such a highly unique interface remains un-reported to date, due to the affinity of the biological component for the target materials, thus presenting unique, new opportunities to modulate the nanosheet interface due to the extended biointerfacial structure. Similar structures were observed with the fatty acid incorporated at the N-terminus; however, a smaller proportion of the biomolecules were present in the vertically-bound state.

Results and discussion

This journal is © The Royal Society of Chemistry 20xx

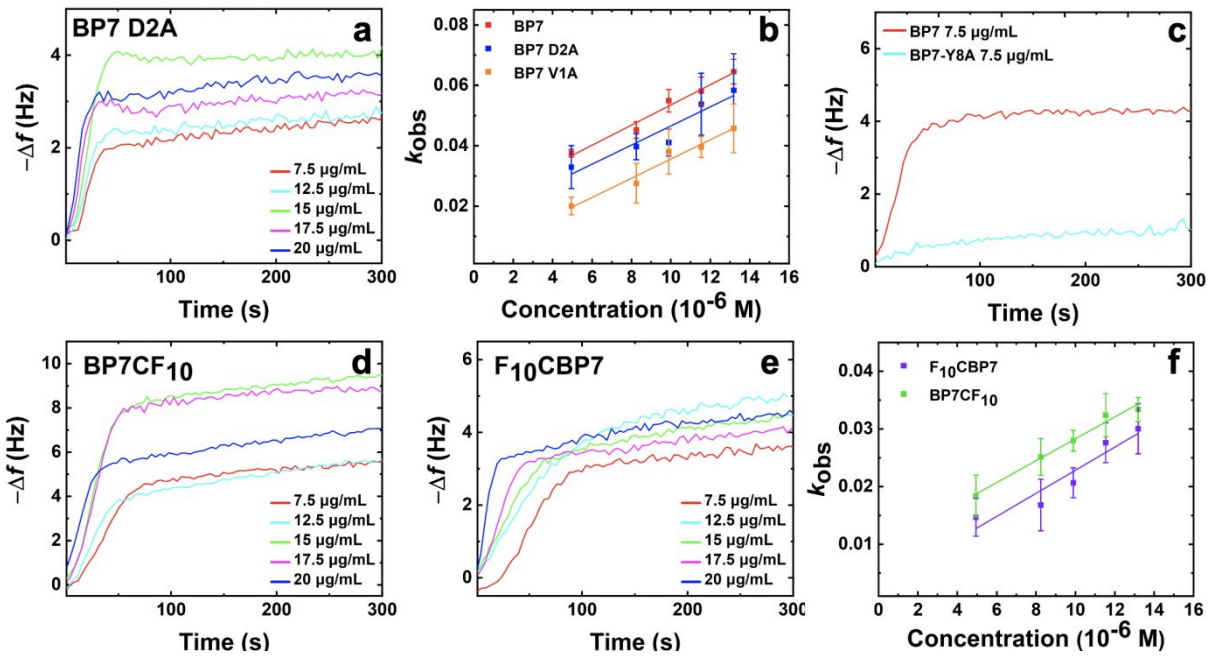

Figure 1. QCM binding analysis for the different peptides studied. Part (a) presents the sensogram for binding of the BP7 D2A mutant on *h*-BN at the indicated peptide concentrations. Part (b) displays a plot of the k_{obs} values as a function of concentration in the QCM analysis to determine the binding free energies. Part (c) compares the binding of BP7 and BP7 Y8A on *h*-BN at 7.5 μg/mL, demonstrating the lack of binding of the mutated peptide. Finally, parts (d-f) present the binding of the fatty acid-modified BP7 peptides with the appropriate sensograms (d-BP7CF$_{10}$ and e-F$_{10}$CBP7) and (f) a plot of their k_{obs} values as a function of peptide concentration.

Table 1. Peptide sequences examined, their free energy of binding to *h*-BN (Δ*G*), and maximum dissipation energy. Red indicates the Ala mutation sites and the fatty acid moiety.

Peptide	Sequence	ΔG (kJ mol^{-1})	Maximum Dissipation Energy (u)
BP7	VDAQSKSYTLHD	-29.5 ± 0.3	0.11
BP7 D2A	VAAQSKSYTLHD	-30.3 ± 4.1	0.22
BP7 Y8A	VDAQSKSATLHD	–	0.17
BP7 V1A	ADAQSKSYTLHD	-33.7 ± 3.0	0.17
BP7CF$_{10}$	VDAQSKSYTLHDCF$_x$	-30.2 ± 2.6	1.81
F$_{10}$CBP7	F$_x$CVDAQSKSYTLHD	-33.3 ± 1.6	0.36

*x: 10-carbon fatty acid

To modulate the affinity and surface adsorbed peptide structure, the BP7 peptide was examined as the parent sequence for binding to *h*-BN. Hanagata and coworkers identified two key residues as being critical for material binding: V1 and Y8.[12] Alternatively, the D2 residue was indicated to have only a minor role in *h*-BN binding. To probe these effects, three mutants, termed BP7 V1A, BP7 D2A, and BP7 Y8A (Table 1), were synthetically prepared with substitutions of the indicated positions by alanine. Hanagata and colleagues previously used these sequences for qualitative evaluation of binding to BNNS;[12] however, the sequences were tagged with an aromatic dye (fluorescein isocthioyanate, FITC) that might have significant implications on the binding affinity, given published studies regarding aromatic/*h*-BN binding strength.[13, 16] In addition, BNNS were employed for their binding studies and not 2D *h*-BN nanosheets; to date, curvature effects on peptide binding are not understood for *h*-BN surfaces, and it is possible this influence may affect binding. Beyond alanine screening at vital positions, incorporation of hydrophobic fatty acid domains of ten carbon chains in length at the N- and C-termini were also examined (termed F$_{10}$CBP7 and BP7CF$_{10}$). To incorporate the fatty acids, cysteine residues were appended at the indicated terminus, which was then used to integrate the maleimide modified fatty acid via thiol/maleimide coupling (ESI, Figure S1).[17] The coupling product was purified via HPLC and confirmed by MALDI-TOF mass spectrometry. Fatty acid incorporation was examined due to the hydrophobic nature of the *h*-BN interface, where the introduction of the hydrophobic domains into the amphipathic peptide could have significant binding implications. Such effects of non-peptide-based sequence modifications are only minimally understood for materials

binding peptides, thus enhancing the value of such information for controlled material production/modification.

The binding free energy (Δ*G*) of the mutants and fatty acid modified peptides was analyzed using QCM measurements. This technique is able to exploit the piezoelectric properties of quartz to measure changes in mass adsorbed at the sensor surfaces via changes in the resonant frequency (Δ*f*). For this analysis, aqueous peptide solutions are flowed over the *h*-BN coated sensors,[13] allowing for peptide to bind the surface, from which the Δ*f* of the system can be monitored. This process is repeated at several different concentrations, where the resultant data (Δ*f* vs time) can be fit using the Langmuir isotherm to extract k_{obs} values at each peptide concentration. Figure 1a presents an example QCM sensogram for the BP7 D2A peptide at the indicated biomolecule concentrations. Note that these data were inverted for a more intuitive interpretation. From a plot of the k_{obs} values at the individual peptide concentrations, fitting of the data linearly can be used to determine the k_a (slope) and k_d (*y*-intercept) from the line of best fit. Using this information, the Δ*G* values for peptide binding to the *h*-BN surface can be determined using standard thermodynamic relations.[14]

From the QCM analysis, the Δ*G* value for each peptide was quantified, as presented in Table 1. For comparison, the parent BP7 sequence was previously determined to have a Δ*G* value of -29.5 ± 0.3 kJ mol^{-1} for binding to *h*-BN.[13] When the same process was employed for the BP7 V1A and BP7 D2A mutants, Δ*G* values of -33.7 ± 3.0 and -30.3 ± 4.1 kJ mol^{-1}, respectively, were noted. Taking the uncertainties into account, such values indicate similar binding strengths relative to the parent sequence, suggesting a negligible change in affinity from these two modifications. For the BP7 Y8A peptide binding analysis, the sequence demonstrated dramatically different results. To this end, when the binding analysis was completed at a 7.5 µg/mL concentration, no significant peptide adsorption was noted (Figure 1c). This is in stark contrast to the other sequences that presented rapid adsorption upon the biomolecule coming into contact with the surface at this concentration. Due to this lack of binding at the concentrations employed with the other sequences, this confirms a substantially diminished affinity for the BP7 Y8A sequence for *h*-BN, thus a Δ*G* value could not be quantified.

For the three peptide mutants, the observed Δ*G* for the BP7 D2A and BP7 Y8A, as compared to the parent, are quite similar to the binding analysis reported by Hanagata and colleagues.[12] Although Δ*G* values were not reported by Hanagata and colleagues, their qualitative binding evaluation indicated a significantly diminished binding strength for the BP7 Y8A on the BNNS surface, compared with the parent BP7. Moreover, relative to BP7, a similar binding strength for the BP7 D2A sequence was observed. The corresponding QCM data presented here are consistent with these findings; however, Hanagata and coworkers reported diminished binding for the BP7 V1A sequence, whereas the current QCM analysis suggests no change in affinity as compared to BP7. Such differences might have arisen from the aromatic dye used by Hanagata and colleagues for the binding analysis.[12] In that sense, the aromatic

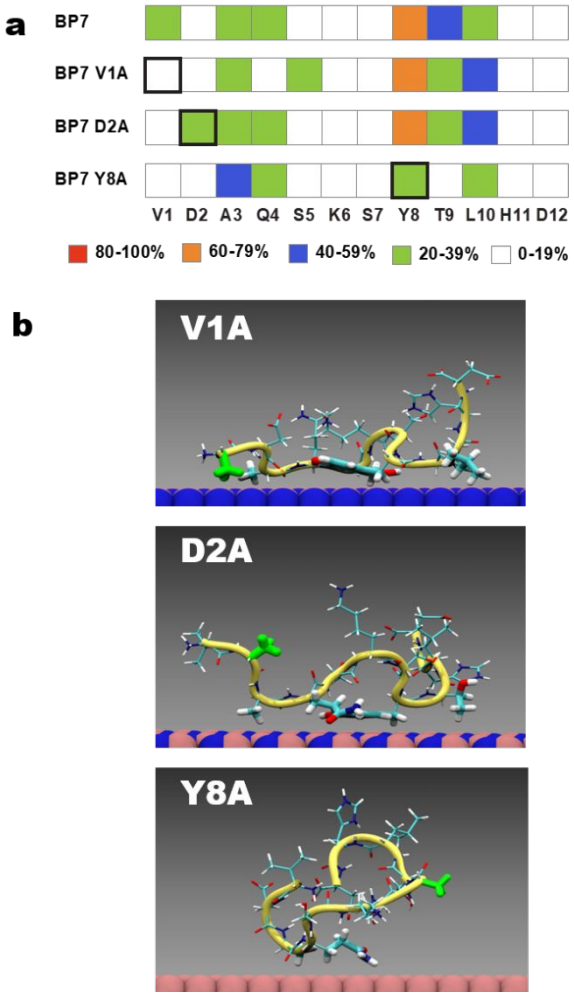

Figure 2. Summary of peptide/surface contact for BP7 mutant sequences. (a) Average residue-surface contact for the parent BP7 and three mutant sequences, predicted from the REST-MD simulations. Black squares highlight Ala mutation sites. (b) Snapshots of the most populated configurations for the three mutant sequences in the surface-adsorbed state. The mutated Ala is highlighted in green, residues in surface contact are highlighted with thicker bonds, water not shown for clarity.

dye may aid in binding to the BNNS surface. In this present study, label-free peptides were employed, thus the quantified value comes directly from the biomolecule without extraneous dye tags.

REST-MD simulations were performed to gain molecular-level insights into the similarities and differences in binding configuration(s) of the mutated sequences in comparison to the parent BP7 peptide. A key analysis of these simulations is the predicted residue-surface contact, as summarized for the parent and all mutants in Figure 2a. Previously published residue-surface contact data for the BP7 parent indicated anchor residues at Y8 and L10, whereas V1 was suggested to only have weak surface contact; in comparison, D2 featured weaker surface contact than V1.[13] Interpretation of the outcomes of the Ala mutation studies can be viewed in terms of enthalpic considerations, and were guided by two pieces of information. First, the naïve (and sometimes inaccurate) assumption that Ala point mutation affects peptide/surface binding *only* at the mutation site, and second, knowledge of the

This journal is © The Royal Society of Chemistry 20xx

predicted amino acid binding free energies on *h*-BN.[16] Regarding the latter, the amino acids Asp and Ala are thought to be a non-binder and a weak binder, respectively, whereas the Tyr amino acid was predicted to bind strongly (no data has been published for the Leu amino acid). For the D2A and Y8A mutants, the predicted residue-surface contact (Figure 2a) confirms the simple assumption about point mutations, and is consistent with the amino acid data. For D2A, this is reflected in the minor changes to the residue-surface contact pattern compared with the parent (Figure 2b). For Y8A, the loss of the strong Tyr anchor resulted in a substantial loss in peptide-surface contact across the entire sequence, consistent with the QCM data and suggesting that the impacts of the point mutation were not localized (Figure 2b).

In contrast, interpretation of the V1A residue-surface contact suggests that Val is, at best, a modest binder for *h*-BN (on par with Ala), when compared with the QCM data, leading to a minimal change in the peptide-surface contact (Figure 2a and b). This would explain the lack of change in the peptide binding free energy compared with the parent BP7 sequence. Furthermore, no amino acid binding data for Val are currently available to provide a benchmark. In this sense, the QCM and REST-MD simulation data are fully consistent. However, as noted earlier, this outcome does not tally with the reduced binding of the FITC-tagged V1A mutant on BNNS, reported by Hanagata and coworkers.[12] It is noted here that FITC conjugation typically is achieved at the N-terminal amine. Previous studies of the impacts of other non-natural conjugates on peptide-surface binding demonstrate that the peptide contact can be profoundly affected, particularly in regions proximal to the conjugation site.[15] The FITC tag could then conceivably affect the Val/surface contact, leading to the inconsistency in the label-free data presented here, and the existing FITC-tagged data reported previously.

QCM analysis of the fatty acid modified BP7 peptide (both F_{10}CBP7 and BP7CF_{10}) was also accomplished to identify the effects of the hydrophobic component on the affinity of the biomolecule to *h*-BN (Figure 1d-f). For these molecules, the F_{10}CBP7 yielded a ΔG value of -33.3 ± 1.6 kJ mol^{-1} while the BP7CF_{10} sequence gave rise to a free energy of binding of -30.2 ± 2.6 kJ mol^{-1}. Such values again signify slightly stronger binding than the parent BP7 where a minor increase in *h*-BN affinity could be observed when the fatty acid was incorporated at the N-terminus (F_{10}CBP7). While the values suggest slightly stronger binding, these indicate that the hydrophobic moiety does not substantially affect binding strength for the target nanosheet surface. Such effects were somewhat surprising due to the hydrophobic nature of *h*-BN; however, these results are consistent with similar effects of fatty-acid-modified materials binding peptides on graphene.[15]

REST-MD simulations were also used to investigate how the presence of the fatty acid modified the molecule-surface binding characteristics. In this instance, both enthalpic and entropic considerations are useful to interpret and guide the comparison between modeling and experiment. The enthalpic influence on binding can be inferred from the residue-surface contact (Figure 3a), which indicates that dramatic differences in the peptide-surface contact mode can be produced depending on fatty acid attachment point. Compared with the BP7 parent, F_{10}CBP7 supports a mixture of up- and down-modulation of residue-surface contact, conferring an overall change in binding enthalpy that is likely close to neutral when also considering the strong surface contact of the fatty acid chain (example binding configuration shown in Figure 3b). It is noted that the N-terminal conjugation has tuned up the Val1/surface contact, which is relevant to the discussion above regarding FITC tag attachment. In contrast, the residue-surface contact for BP7CF_{10} is remarkably diminished, with only the Tyr8 and Leu10 anchor residues supporting any substantive contact at all, both of which are modest at best (example binding configuration shown in Figure 3c). Here, the fatty acid chain features the strongest surface contact for this biomolecule, although the fatty acid contact itself is weaker than that observed for F_{10}CBP7. Furthermore, as reported in a previous study, both molecules support a number of surface-adsorbed and surface-detached states in the simulations. The ratio of the number of these two states (on:off) can be used as an approximate indicator of the binding constant; in this case these are 0.73:0.27 and 0.87:0.13 for BP7CF_{10} and F_{10}CBP7, respectively. A full breakdown of the on:off states in terms of F_{10} contact and peptide contact are provided in Figure S2, ESI. Therefore, on enthalpic considerations alone, it is expected that F_{10}CBP7 would bind more strongly to *h*-BN.

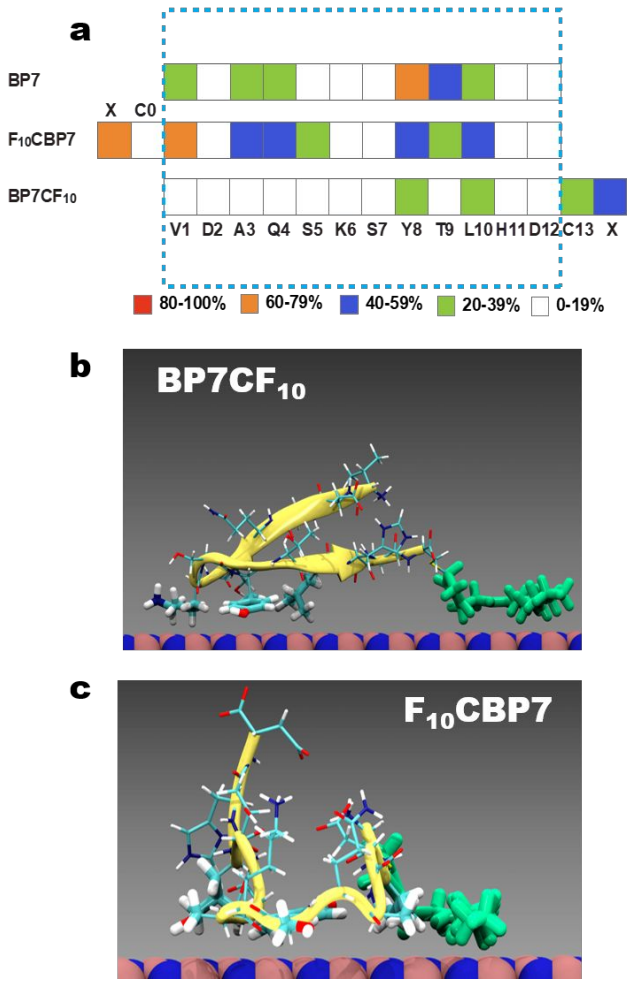

Figure 3. Summary of peptide/surface contact for the BP7/fatty acid bioconjugates. (a) Average residue-surface contact for the parent BP7, F_{10}CBP7 and BP7CF_{10} predicted from the REST-MD simulations. (b), (c) Snapshots of the most populated configurations for the two bioconjugates in the surface-adsorbed state. The fatty acid is highlighted in green, residues in surface contact are highlighted with thicker bonds, water not shown for clarity.

However, as previously reported,[14, 15] entropic considerations can also play a role in contributing to the free energy of binding. In this instance, a peptide may only have a number of weak enthalpic contacts, but consequently may support a large number of different binding conformations in achieving these contacts, hence collectively leading to a substantial adsorption free energy. Here, this entropic contribution, S_{conf}, has been calculated for the surface-adsorbed conformational ensembles of BP7CF_{10} and F_{10}CBP7 predicted from the REST-MD simulations, following previously reported methods (summarized in 'Computational Details', ESI).[15, 18, 19] S_{conf} values of 4.20 and 5.27 were estimated for F_{10}CBP7 and BP7CF_{10}, respectively. Both of these values are high compared with previously reported values for a graphene-binding peptide bioconjugate P1CF_{10}/F_{10}CP1 adsorbed on graphene,[15] and the difference reported here is genuinely indicative of a substantial enhancement in the entropic contribution for BP7CF_{10}, relative to F_{10}CBP7, which offers a plausible explanation for their similarities in adsorption free energy (Table 1). The modeling

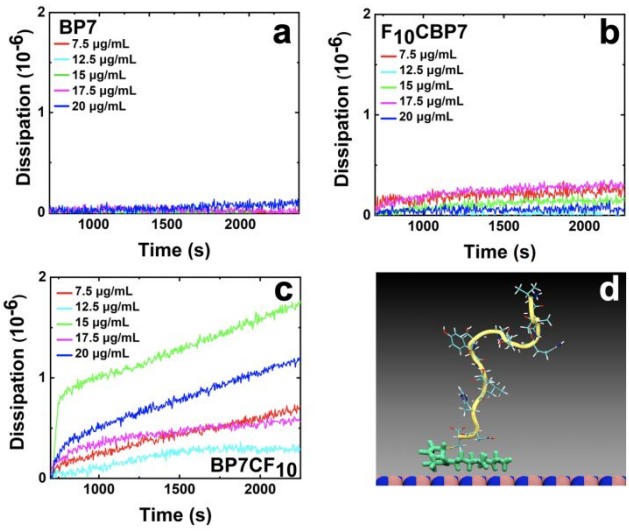

Figure 4. Measurement of dissipation energies for the binding of (a) BP7, (b) F_{10}CBP7, and (c) BP7CF_{10} on *h*-BN. Part (d) presents an example of an upright binding configuration, mediated by fatty acid/surface contact, predicted for BP7CF_{10} from the REST-MD simulations. Fatty acid highlighted in green, water not shown for clarity.

data therefore suggest F_{10}CBP7 and BP7CF_{10} are enthalpically- and entropically-driven *h*-BN binders, respectively.

This entropic contribution led to remarkable differences in the physical properties of the bioconjugate overlayers at the aqueous *h*-BN interface. While QCM is capable of determining the ΔG values for each peptide overlayer adsorbed to the *h*-BN surface, it is also capable of quantifying the dissipation energy of the biointerface that is formed. This dissipation energy reflects the viscoelasticity of the biointerface detected using the QCM analysis, which is related to the degree of mechanical softness of the biomolecular adlayer. To date, across multiple compositions of materials, only low-viscoelastic adlayers have been observed for interfaces between materials-binding peptides and solid surfaces.[14, 15, 18] Such adlayers typically give rise to negligible dissipation energy, which was observed here for the BP7 (Figure 4a) and the mutated sequences; however, for the fatty acid modified species, dramatically different results were noted. For F_{10}CBP7, a slight increase in the dissipation energy was indicated over the time frame of the study (Figure 4b) suggesting a modest increase in the viscoelasticity of the adlayer; however, for the BP7CF_{10} peptide (Figure 4c), a substantial increase in dissipation energy was observed. For perspective, the maximum dissipation energy determined for the parent BP7 during the QCM analysis on *h*-BN was 0.11; however, for the same analysis using the BP7CF_{10}, the dissipation energy was 1.81. This indicates that modification of the peptide with the fatty acid can have substantial implications on the adlayer morphology, giving rise to dramatic changes in the surface overlayer viscoelasticity. Furthermore, positioning of the fatty acid within the sequence (*i.e.* at either terminus) also appears to produce a remarkable difference in the viscoelasticity of this overlayer.

The outcomes of the REST-MD simulations suggest an explanation for this remarkable difference. To identify this feature, it was initially noticed from visual inspection of the adsorbed-state trajectories that BP7CF_{10} supported a

This journal is © The Royal Society of Chemistry 20xx

considerable number of adsorbed states in which the molecule was surface-attached chiefly *via* the F_{10} chain, leading to an unusual, perpendicular (upright) binding configuration where the peptide domain was mostly detached from the surface. An example of this upright binding state for $BP7CF_{10}$ is provided in Figure 4d. On visual inspection alone, these states were not as apparent in the corresponding trajectory for $F_{10}CBP7$. Quantification of the number of upright binding states was performed for both the $BP7CF_{10}$ and $F_{10}CBP7$ REST-MD trajectories (details in ESI 'Peptide Orientation Analysis') confirmed this effect; 43% of the total frames in the $BP7CF_{10}$ trajectory were classified as upright states, compared with 13% for $F_{10}CBP7$. It is thus postulated that this high proportion of upright states could explain the enhanced viscoelastic response observed for the $BP7CF_{10}$ overlayer. Further explanation regarding the most populated configuration shown in Figure 3c is warranted. In this instance, even the most populated structure of $BP7CF_{10}$ only shares an extremely small percentage of the total conformational ensemble (4%, details in ESI, 'Clustering Analysis'). There are numerous different types of upright states, each with similarly small (less than 4%) populations; collectively, these add up to the 43% of upright states quoted above.

The underlying cause for this difference in the proportion of upright states is attributed to modulation of the anchor Tyr8 residue surface contact. The role of Tyr8 as an anchor residue was demonstrated in the mutation studies. Attachment of the fatty acid at the C-terminus appears to down-modulate Tyr8/surface engagement (Figure S4, ESI), releasing this anchor point and facilitating the upright (peptide-detached) configurations. In contrast, the Tyr8/surface contact is less affected by fatty acid attachment at the N-terminus, compared with the parent BP7 (Figure 3), resulting in a greater fraction of peptide-anchored states and therefore fewer upright states. It is proposed that a proximity effect gives rise to this difference in Tyr8 contact. To elaborate, the C-terminal conjugate has the fatty acid closer to Tyr8 (a 5 residue separation), whereas the N-terminal conjugate has the fatty acid and Tyr8 separated by 8 residues, which could conceivably be too distant (in sequence space) to exert substantial influence.

The influence of inter-chain interactions on this hypothesis cannot be resolved by the current, single-molecule REST-MD simulations. As a prelude to a deeper investigation, preliminary standard MD simulations of 100 ns duration were performed on an overlayer of either $BP7CF_{10}$ or $F_{10}CBP7$ adsorbed at the aqueous *h*-BN interface. The initial configurations of these layers were populated with likely conformations predicted from the REST-MD simulations. These overlayer simulations revealed very similar properties compared to the single-chain predictions. In brief, and illustrated in Figure S5, ESI, the $BP7CF_{10}$ overlayer showed a substantially increased layer thickness due to upright states and featured a highly clustered layer morphology, whereas the $F_{10}CBP7$ overlayer was quantifiably less thick and featured fewer upright states (which did not protrude to the same extent as the $BP7CF_{10}$ chains). Full details are provided in the ESI. The inter-chain interactions in these layers will be investigated in future work.

Conclusion

In conclusion, the current work demonstrates that chemical modification of materials-binding peptides can be exploited to dramatically switch the surface adsorbed configuration of the biomolecular overlayer. This was demonstrated through the incorporation of a fatty acid domain within an *h*-BN binding peptide (BP7), where the attachment point of the fatty acid has a substantial influence over the binding orientation and subsequent packing of these molecules on the *h*-BN surface. Most remarkably, switching from a flat overlayer structure to a conformation where the peptide is extended from the nanosheet surface and presented to solution was achieved, to generate an unusual highly viscoelastic surface. Furthermore, this upright binding state presents the N-terminus outwards from the surface, providing a readily-accessible attachment point for subsequent and further bioconjugation (*e.g.* a secondary materials-binding peptide or non-natural moiety). An explanation based on the proximity of the anchor residue to the fatty acid attachment point provides guidance to generalizing this phenomenon for other *h*-BN binding peptides. This ability to controllably switch peptide/surface binding orientation from horizontal to upright has not been reported in the literature to date, and opens significant new avenues in biotic/abiotic interface design, particularly for future device materials. Molecules that vary the peptide sequence, fatty acid chain length, etc. would be interesting to analyze for this viscoelasticity effect, and will be the subject of future work.

Experimental

Replica-Exchange with Solute Tempering Molecular Dynamics (REST-MD) Simulations.

REST-MD simulations[20, 21] were used to predict the Boltzmann-weighted conformational ensemble for the three Ala mutants (BP7 V1A, BP7 D2A, and BP7 Y8A), and the two fatty acid bioconjugates $BP7CF_{10}$ and $F_{10}CBP7$, under aqueous conditions in the presence of the *h*-BN surface. Two periodic *h*-BN surfaces were placed in an orthorhombic periodic simulation cell of lateral dimensions ~7.5 × ~6.5 nm, with a cell dimension vertical to the graphene plane of 12 nm, with a vertical spacing (between the parallel *h*-BN sheets) of 8 nm. This 8 nm vertical space between the two sheets was filled with liquid water, along with one chain of the relevant biomolecule. Periodic boundary conditions were applied in all three principal directions. All simulations were performed in the Canonical (NVT) ensemble, at a thermal temperature of 300 K. Similar to the procedure reported previously for interfacial REST-MD simulations of peptide bio-conjugates,[15] 16 replicas were used. REST-MD trajectories were of 20 ns duration (amounting to 16 × 20 ns = 0.32 μs of nominal total simulation time). The initial structures of the 16 replicas included a wide range of secondary structure motifs for the peptide region, including α-helices, β-turns, polyproline II, and random coil structures. A previously-tested force-field combination[13] was used comprising CHARMM22*[22, 23] for the peptides (with parameter modifications to describe the maleimide-mediated fatty acid

linkage, as reported previously[24]) and the BoNi-CHARMM force-field for *h*-BN,[16] along with the modified TIP3P[25, 26] force-field for water. Complete details of these simulations and their analyses are provided in the ESI.

Materials.

Decanoyl chloride and sodium dodecyl sulfate (SDS) were purchased from Sigma Aldrich while dichloromethane (DCM) was acquired from Macron Fine Chemicals. Ethyl ether, triethylamine (TEA) and *N*,*N*-dimethylformamide (DMF) were obtained from EMD Milipore Corporation. *N*-(2-aminoethyl)-maleimide hydrochloride was purchased from TCI and ammonium persulfate $(NH_4)_2S_2O_8$ was obtained from BDH Chemicals. The peptides used were commercially purchased from Genscript. The copper foil containing a single layer of *h*-BN was obtained from Grolltex, while the thermal release tape was purchased from Semiconductor Equipment Corporation. The Au sensors used in QCM experiments were sourced from Biolin Scientific. During all experiments, deionized water (18.2 MΩ•cm) was used and all chemicals were used as acquired.

Synthesis of Maleimide Modified Fatty Acid.

In a vial, 25.0 mg of decanoyl chloride is added to 5.0 mL of DCM under stirring and then cooled to 0-5 °C. In a separate vial, 48.1 mg of *N*-(2-aminoethyl)-maleimide hydrochloride and 94.71 µL of triethylamine (TEA) was added to 5.0 mL of DCM. The second mixture was slowly added to the first mixture in a dropwise manner under N_2 atmosphere. The reaction was brought back to room temperature and allowed to proceed overnight. Next, the reaction solution was evaporated, and the resulting solid was dissolved in 50.0 mL of water, followed by vacuum-filtration to remove any water soluble impurities. The collected solid was dissolved in 50.0 mL of ethyl ether, followed by vacuum-filtration to remove the insoluble impurities. The collected solution was subjected to evaporation to obtain the final product which was confirmed by a Bruker Avance 400 MHz ^{1}H NMR and a Bruker microTOF-Q II ESI-TOF mass spectrometer.

Peptide/Fatty Acid Coupling.

For this reaction, 7.03 mg of the synthesized maleimide modified fatty acid was dissolved in 5.0 mL of DMF. In a separate vial, 25.0 mg of peptide with a cysteine appended on either the N- or C-terminus was dissolved in 5.0 mL of DMF. The second solution was slowly added to the first at room temperature and was stirred for 3-4 days at 800 rpm. The resulting fatty acid modified peptide was washed with 30 mL of ethyl ether, centrifuged for 5 min at 7800 rpm, and the supernatant was removed. This process was repeated three times. The obtained product was purified by reverse phase HPLC (Waters 2489 UV-vis detector and Waters 600 controller) and confirmed by a Bruker autoflex speed LRF MALDI-TOF mass spectrometer.

QCM h-BN Sensor Fabrication.

A Cu foil prepared with a single layer of *h*-BN on the surface was purchased and used for the fabrication of *h*-BN coated QCM sensors using previous methods.[13] The *h*-BN layer on the Cu foil was transferred onto thermal release tape and then subjected to an UV-ozone treatment for 5 min. The system was then etched with $(NH_4)_2S_2O_8$ (100 mg/mL) for 3 h to remove the metal foil, after which it was washed with DI water and dried with N_2 gas. Adhesion of the *h*-BN thermal release tape to Au QCM sensors was done at room temperature and then thermally released by heating to 125 °C on a hotplate.

QCM Analysis.

The peptide concentrations used varied from a range of (7.5-20 µg/mL). Before each run, the QCM *h*-BN sensors were exposed to 5 min UV-ozone treatment. The sensors were then placed in the QCM, in which DI water was flowed for 30 min, followed by 4% SDS for 30 min, and finally 30 min of DI water at a flow rate 150 µL/min. The measurements started with a 10 min run of DI water, followed by 30 min flow of peptide solution at 22.5 °C.

Corresponding Author

*To whom correspondence should be addressed: TRW – tiffany.walsh@deakin.edu.au; MRK – knecht@miami.edu

Author Contributions

The manuscript was written through contributions of all authors. All authors have given approval to the final version of the manuscript.
‡These authors contributed equally.

Funding Sources

This material is based upon work supported by the Air Force Office of Scientific Research, Grant FA9550-18-1-0329.

Conflicts of interest

There are no conflicts to declare.

Acknowledgements

RJ and TRW thank the National Computational Infrastructure, Canberra, and the Pawsey Supercomputing Centre, Perth, for provision of computational resources under the NCMAS scheme.

References

1. Y. Zhang, X. Weng, H. Li, H. Li, M. Wei, J. Xiao, Z. Liu, M. Chen, Q. Fu and X. Bao, *Nano Lett.*, 2015, **15**, 3616-3623.
2. V. Kumar, K. Nikhil, P. Roy, D. Lahiri and I. Lahiri, *RSC Adv.*, 2016, **6**, 48025-48032.
3. A. F. Khan, D. A. C. Brownson, E. P. Randviir, G. C. Smith and C. E. Banks, *Anal. Chem.*, 2016, **88**, 9729-9737.
4. R. Han, F. Liu, X. Wang, M. Huang, W. Li, Y. Yamauchi, X. Sun and Z. Huang, *J. Mater. Chem. A*, 2020, **8**, 14384-14399.

This journal is © The Royal Society of Chemistry 20xx

5. K. Zhang, Y. Feng, F. Wang, Z. Yang and J. Wang, *J. Mater. Chem. C*, 2017, **5**, 11992-12022.
6. W. Luo, Y. Wang, E. Hitz, Y. Lin, B. Yang and L. Hu, *Adv. Funct. Mater.*, 2017, **27**, 1701450.
7. L. H. Li, J. Cervenka, K. Watanabe, T. Taniguchi and Y. Chen, *ACS Nano*, 2014, **8**, 1457-1462.
8. A. Merlo, V. R. S. S. Mokkapati, S. Pandit and I. Mijakovic, *Biomater. Sci.*, 2018, **6**, 2298-2311.
9. T. R. Walsh and M. R. Knecht, *Bioconjug. Chem.*, 2019, **30**, 2727-2750.
10. Y. Cui, S. N. Kim, S. E. Jones, L. L. Wissler, R. R. Naik and M. C. McAlpine, *Nano Lett.*, 2010, **10**, 4559-4565.
11. M. S. Mannoor, H. Tao, J. D. Clayton, A. Sengupta, D. L. Kaplan, R. R. Naik, N. Verma, F. G. Omenetto and M. C. McAlpine, *Nat. Commun.*, 2012, **3**, 763.
12. H. Zhang, T. Yamazaki, C. Zhi and N. Hanagata, *Nanoscale*, 2012, **4**, 6343-6350.
13. N. Brljak, A. D. Parab, R. Rao, J. M. Slocik, R. R. Naik, M. R. Knecht and T. R. Walsh, *Chem. Commun.*, 2020, **56**, 8834-8837.
14. Z. Tang, J. P. Palafox-Hernandez, W.-C. Law, Z. E. Hughes, M. T. Swihart, P. N. Prasad, M. R. Knecht and T. R. Walsh, *ACS Nano*, 2013, **7**, 9632-9646.
15. A. D. Parab, A. Budi, N. Brljak, M. R. Knecht and T. R. Walsh, *Adv. Mater. Interfaces*, 2020,**n/a**, 2001659.
16. A. Budi and T. R. Walsh, *Langmuir*, 2019, **35**, 16234-16243.
17. A. D. Parab, A. Budi, J. M. Slocik, R. Rao, R. R. Naik, T. R. Walsh and M. R. Knecht, *J. Phys. Chem. C*, 2020, **124**, 2219-2228.
18. J. P. Palafox-Hernandez, Z. Tang, Z. E. Hughes, Y. Li, M. T. Swihart, P. N. Prasad, T. R. Walsh and M. R. Knecht, *Chem. Mater.*, 2014, **26**, 4960-4969.
19. Z. E. Hughes and T. R. Walsh, *J. Mater. Chem. B*, 2015, **3**, 3211-3221.
20. T. Terakawa, T. Kameda and S. Takada, *J. Comput. Chem.*, 2011, **32**, 1228-1234.
21. L. B. Wright and T. R. Walsh, *Phys. Chem. Chem. Phys.*, 2013, **15**, 4715-4726.
22. A. D. MacKerell, D. Bashford, M. Bellott, R. L. Dunbrack, J. D. Evanseck, M. J. Field, S. Fischer, J. Gao, H. Guo, S. Ha, D. Joseph-McCarthy, L. Kuchnir, K. Kuczera, F. T. K. Lau, C. Mattos, S. Michnick, T. Ngo, D. T. Nguyen, B. Prodhom, W. E. Reiher, B. Roux, M. Schlenkrich, J. C. Smith, R. Stote, J. Straub, M. Watanabe, J. Wiórkiewicz-Kuczera, D. Yin and M. Karplus, *J. Phys. Chem. B*, 1998, **102**, 3586-3616.
23. S. Piana, K. Lindorff-Larsen and David E. Shaw, *Biophys. J.*, 2011, **100**, L47-L49.
24. J. P. Palafox-Hernandez, C.-K. Lim, Z. Tang, K. L. M. Drew, Z. E. Hughes, Y. Li, M. T. Swihart, P. N. Prasad, M. R. Knecht and T. R. Walsh, *ACS Appl. Mater. & Interfaces*, 2016, **8**, 1050-1060.
25. W. L. Jorgensen, J. Chandrasekhar, J. D. Madura, R. W. Impey and M. L. Klein, *J. Chem. Phys.*, 1983, **79**, 926-935.
26. E. Neria, S. Fischer and M. Karplus, *J. Chem. Phys.*, 1996, **105**, 1902-1921.

This journal is © The Royal Society of Chemistry 20xx